ACS APPLIED MATERIALS & INTERFACES

Research Article

www.acsami.org

Efficient Photocatalytic Hydrogen Production by Platinum-Loaded Carbon-Doped Cadmium Indate Nanoparticles

Jason M. Thornton and Daniel Raftery*

Department of Chemistry, Purdue University, 560 Oval Drive, West Lafayette, Indiana 47907, United States

ABSTRACT: Undoped and carbon doped cadmium indate ($CdIn_2O_4$) powders were synthesized using a sol–gel pyrolysis method and evaluated for hydrogen generation activity under UV–visible irradiation without the use of a sacrificial reagent. Each catalyst powder was loaded with a platinum cocatalyst in order to increase electron–hole pair separation and promote surface reactions. Carbon-doped indium oxide and cadmium oxide were also prepared and analyzed for comparison. UV–vis diffuse reflectance spectra indicate the band gap for C-$CdIn_2O_4$ to be 2.3 eV. C-doped In_2O_4 showed a hydrogen generation rate approximately double that of the undoped material. When compared to platinized TiO_2 in methanol, which was used as a control material, C-$CdIn_2O_4$ showed a 4-fold increase in hydrogen production. The quantum efficiency of the material was calculated at different wavelength intervals and found to be 8.7% at 420–440 nm. The material was capable of hydrogen generation using visible light only and with good efficiency even at 510 nm.

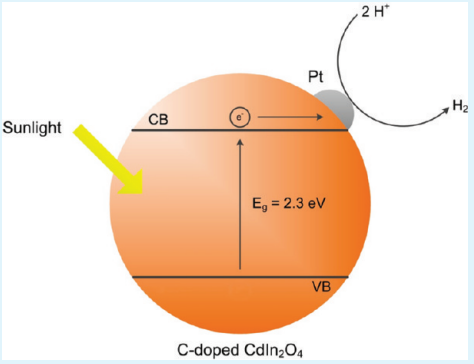

KEYWORDS: *$CdIn_2O_4$, photocatalysis, solar hydrogen conversion, hydrogen generation, C-doping*

INTRODUCTION

Concerns over global climate change and growing energy consumption have caused an increased interest in alternative energy research. Energy needs are expected to double the current consumption rate by the year 2050.[1] Of all the alternative energy solutions, such as biomass, wind, hydroelectric, and geothermal, solar is the only solution that is potentially capable of providing sufficient energy to satisfy global demand.[2] Photoelectrochemical generation of hydrogen from the solar-driven splitting of water has gained considerable attention because of its ability to provide a clean and renewable energy source.[3] Development of photocatalysts for overall water splitting has been under investigation since Fujishima and Honda first demonstrated the ability of TiO_2 to generate H_2 and O_2 from water under UV irradiation in the early 1970s.[4] A variety of photocatalysts, such as TiO_2, Fe_2O_3, WO_3, and ZnO[5−13] have been studied for their ability to split water. Materials focusing on oxygen evolution have also garnered considerable attention, such as those based on Mn and analogs to photosystem II.[14,15] Metal oxides such as these provide good chemical stability but suffer from the disadvantage of a relatively large bandgap, which generally requires UV light excitation. Many semiconductors with smaller band gaps that allow for a wider range of wavelengths to be absorbed have the disadvantage of being unstable photochemically. Band gap reduction of metal oxides by impurity doping allows for absorption of light in the visible region with the potential for increased photocatalytic activity while maintaining good stability. Anion doping has shown to be a promising approach for band gap modification in metal oxide semiconductors.[16−19] The use of mixed metal oxides for band gap reduction has also gained interest.[20,21]

One such material that has shown potential for good photoelectrochemical performance is cadmium indate.[22] Undoped $CdIn_2O_4$ has good electrical conductivity, is transparent in the visible range range due to a wide band gap (~2.7 eV) and has high chemical stability.[23] Our group recently showed that the introduction of carbon into the crystal lattice reduces the band gap to 2.4 eV and increases the total photocurrent contribution of the visible response from 21% for the undoped electrode to 33% after C-doping.[22]

In this study, we report on direct H_2 production by C-doped $CdIn_2O_4$ in aqueous medium adjusted to pH 14 without the addition of any sacrificial reagents. The ratio of Cd to In, carbon doping concentration and calcination temperature were all optimized in a previous study.[22] In this study, we present a simple sol–gel pyrolysis method for catalyst synthesis and Pt cocatalyst loading by photodeposition to prepare the Pt-loaded C-$CdIn_2O_4$ material. The wavelength dependent quantum conversion efficiency of photons to generated H_2 is reported.

EXPERIMENTAL SECTION

Indium(III) nitrate hydrate ($In(NO_3)_3{\cdot}5H_2O$), cadmium(II) nitrate hydrate ($Cd(NO_3)_2{\cdot}6H_2O$), acetylacetone and hexachloroplatinic acid hydrate ($H_2PtCl_6{\cdot}xH_2O$) were obtained from Sigma-Aldrich. Glucose, ammonium hydroxide and potassium hydroxide were obtained from Mallinckrodt. All chemicals were used without further purification.

Received: January 17, 2012
Accepted: April 20, 2012
Published: May 2, 2012

The catalyst powder synthesis for each material began with a solution containing the required metal ions. The C-doped cadmium indate solution was prepared using a 9:1 by volume solution of MeOH:H_2O with initial total volume of 10 mL that contained 1.00 M indium nitrate, 0.5 M cadmium nitrate, 3.0 M acetylacetone, and allowed to stir for 30 min. Ammonium hydroxide was added to the solution (final concentration 3.0 M), followed by additional stirring for 30 min. Lastly, glucose was added (final concentration 0.15 M). The undoped $CdIn_2O_4$ solution was prepared in the same manner but without the addition of glucose. The C-doped In_2O_3 solution was also prepared in the same manner except for the addition of cadmium nitrate. CdO was prepared using a 1.0 M solution of cadmium nitrate in methanol. All solutions were thoroughly stirred for 30 min after the last addition of reactants, and then the solvent was allowed to slowly evaporate on a hot plate overnight. The crystalline material that formed was converted to the metal oxide by calcination in air at 550 °C for 3 h with an initial heating rate of 3 °C/min.

Pt was deposited onto the surface for use as a cocatalyst using a modified photodeposition method.[24] A 1:1 solution by volume of MeOH:H_2O was used to suspend approximately 0.50 g unloaded catalytic powder and an appropriate volume of a hexachloroplatinic acid solution was added to give the desired loading of Pt by percent weight. The solution was stirred vigorously while being irradiated with UV light for 3 h to reduce the H_2PtCl_6 to platinum metal. The catalyst was then washed and dried overnight at 120 °C, resulting in the final Pt loaded catalytic powder. For reference, a sample of 0.3 wt % Pt-loaded P25 TiO_2 (Degussa) was prepared using the same photodeposition method.

XRD analysis was performed on a Bruker D8 Focus X-ray diffractometer employing Cu Kα radiation over the range of $20° \leq 2\theta \leq 80°$. The surface morphologies of the powdered photocatalysts were characterized using SEM imaging on a FEI NOVA nanoSEM scanning electron microscope. UV–vis absorption spectra were acquired using a Cary Bio300 Varian spectrophotometer.

Photocatalytic hydrogen generation experiments were carried out using a 300 W xenon arc lamp as the light source and an AM1.5 filter to match the solar spectrum. A water filter was used to remove IR energy and reduce overheating. The reaction chamber consisted of a sealed cylindrical aluminum cell with a quartz window on the top. The catalytic powder and aqueous solution were isolated from the cell in a pyrex dish. For the H_2 generation experiments, 0.05 g of each catalytic powder was used with the exception of the TiO_2 samples in which 0.1 g of catalyst was used; the small amount used allowed for the powder mass to be the limiting factor in the amount of hydrogen generated. The photocatalytic powders were suspended in 10 mL of ultrapure water (18 MΩ) from a Barnstead EASYpure II water purification system, and the pH of the solution was adjusted to 14 using potassium hydroxide. The reaction solution was degassed prior to each experiment to remove any dissolved O_2 and N_2. No sacrificial agents were added to the solution with the exception of 10% methanol by volume to the solution containing platinized TiO_2. Samples were taken from the gas-phase volume above the aqueous solution containing the catalytic powder and analyzed using an in line SRI Instruments 310C gas chromatograph with a column temperature of 30 °C and a flow gas pressure of 40 psi. The obtained peak area was used to calculate the number of moles of H_2 produced at each time point, and then the area versus time plot was fitted using linear regression. The slope of the resulting line was used to represent the photocatalytic generation rate for each of the materials examined.

A second set of experiments were conducted on the optimized C-doped $CdIn_2O_4$ material to measure the quantum efficiency. For these measurements, individual wavelength regions were selected using a series of bandpass filters (Thor Laboratories, FB series, 10 nm full width at half max transmission) and the filtered light outputs were measured using a calibrated silicon photodiode (Thor Laboratories, PM100D with S121C Detector) and converted to photon flux. In these experiments, an excess amount of powder was used to allow for the light to be the limiting factor in the H_2 generation reaction.

RESULTS AND DISCUSSION

The XRD patterns of C–In_2O_3, C–$CdIn_2O_4$,and CdO were collected on both the unloaded and Pt-loaded samples and showed the expected peaks for all three oxides (Figure 1). The

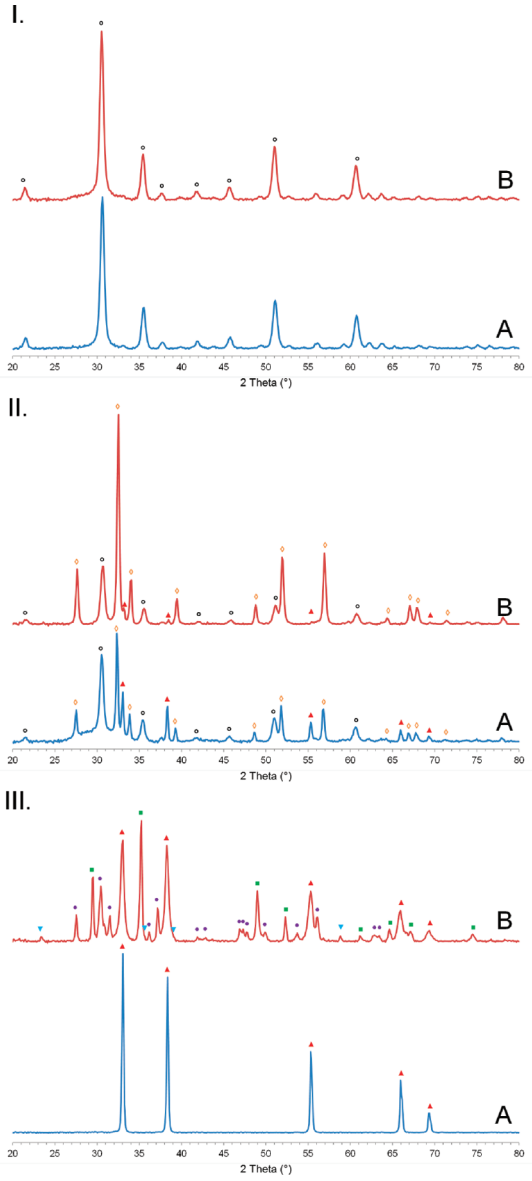

Figure 1. X-ray diffraction patterns for the (A) unloaded and (B) platinum loaded photocatalysts: (I) C–In_2O_3, (II) C-$CdIn_2O_4$, and (III) CdO. C-doped In_2O_3 only showed the expected peaks, corresponding to a cubic structure. (○) In_2O_3, (◇) $CdIn_2O_4$, (▲) CdO, (▼) $Cd_{0.3}Pt_3O_4$, (■) $Cd(OH)_2$, and (●) γ-$Cd(OH)_2$.

cocatalyst loaded samples showed no signs of Pt metal in the diffraction pattern; however, the samples containing Cd did show a reduction in the CdO peak intensity after Pt deposition. C-doped In_2O_3 showed no differences between the unloaded and platinum loaded samples. No differences were observed between the undoped and C-doped $CdIn_2O_4$ samples, and therefore only the doped form is shown in the figure. Both the undoped and C-doped $CdIn_2O_4$ samples showed signs of three cubic phases in the diffraction pattern: In_2O_3, CdO, and $CdIn_2O_4$. In the Pt-loaded samples, all three phases were still apparent, with the In_2O_3,and $CdIn_2O_4$ phases being unchanged

dx.doi.org/10.1021/am300093t | ACS Appl. Mater. Interfaces 2012, 4, 2426–2431

in intensity and the CdO contribution showing a large reduction. This suggests that the CdO interacts with the Pt during deposition. To confirm this effect, a sample of Pt-loaded CdO (0.25 wt %) was prepared and diffraction patterns were collected before and after the loading procedure. Unloaded CdO exhibited the expected diffraction pattern, but the Pt-loaded sample showed not only the original CdO phase but peaks corresponding to two forms of cadmium hydroxide and trace amounts of a cadmium platinum oxide phase were also present. The peaks associated with cadmium hydroxide displayed two forms; $Cd(OH)_2$ and γ-$Cd(OH)_2$, which correspond to the hexagonal and monoclinic forms of the structure, respectively.

The traces of the cadmium platinum oxide phase match the X-ray line positions of the most dominate peaks in $Cd_{0.3}Pt_3O_4$.[25] The X-ray diffraction patterns were used to calculate the particle sizes for each of the powders using the Scherrer equation.[26] The results showed crystal sizes of 14, 26, 24, and 34 nm for C-doped In_2O_3, undoped $CdIn_2O_4$, C-doped $CdIn_2O_4$, and CdO, respectively.

To determine the optical absorption, UV−vis diffuse reflectance and the transformed spectra for the C-$CdIn_2O_4$, $CdIn_2O_4$, CdO, and C−In_2O_3 platinum loaded catalytic powders were acquired (Figure 2). C-doped $CdIn_2O_4$ shows increased absorption over the undoped material in both the visible and the ultraviolet regions despite an onset of absorption for both materials around 600 nm. Assuming the materials are all indirect band gap semiconductors, the modified Kubelka−Munk function, $[F(R)E]^{1/2}$, can be plotted against the excitation energy, E, to determine the band gap.[27]

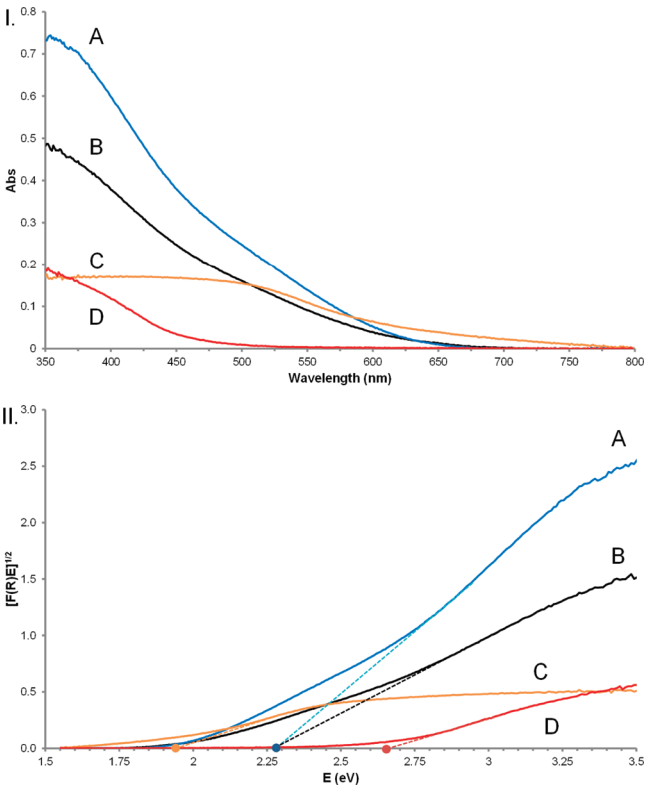

Figure 2. UV−vis (I) diffuse reflectance and (II) transformed spectra of (A) C-$CdIn_2O_4$, (B) $CdIn_2O_4$, (C) CdO, and (D) C−In_2O_3. In the transformed spectra, the dotted lines represent the extrapolated linear regions used to estimate the indirect semiconductor band gap.

The estimated band gap energies are 2.3 eV for C−$CdIn_2O_4$, 2.3 eV for $CdIn_2O_4$, 1.95 eV for CdO, and 2.65 eV for C−In_2O_3. The values for C−$CdIn_2O_4$, $CdIn_2O_4$, and CdO are lower than our previously published results. We attribute the reduction to the difference in synthesis technique, i.e., spray pyrolysis versus the current sol−gel pyrolysis method used[22] to produce the catalytic powders. The band gap value for the carbon-doped In_2O_3 matches very closely with our previous results.[18] Pure $CdIn_2O_4$ is transparent in the visible region but phase impurity of the material, as we observed in the XRD pattern, can lead to a lower band gap. Reports have shown that the pure-phase polycrystalline materials lead to larger optical band gaps.[28] For example, in the analogous material Cd_2SnO_4, mostly polycrystalline films have a band gap near 3.0 eV while high quality single-phase films have band gaps as large as 3.7 eV.[28−30]

SEM images were acquired to determine surface morphology of both the unloaded (Figure 3a,c,e) and Pt-loaded (Figure 3b,d,f) versions of $CdIn_2O_4$, C-doped $CdIn_2O_4$ and CdO powders as well as Pt-loaded C-doped In_2O_3 (Figure 3g). The unloaded $CdIn_2O_4$ (Figure 3a) sample exhibited a well-defined cubic structure, while the unloaded C-doped $CdIn_2O_4$ (Figure 3c) sample exhibited a less defined structure. The unloaded CdO (Figure 3e) showed an amorphous structure. Interestingly, the Pt-loaded samples show nanosized fibers coating the surface of the particles. We have determined that these fibers result from the Pt deposition in the presence of Cd since this effect was not witnessed on platinized C-doped In_2O_3. This conclusion is also supported by the reduction in the XRD peak intensity observed in the Cd containing samples after Pt deposition. In the case of the $CdIn_2O_4$-based samples, the underlying morphology was unchanged between Pt-loaded and nonloaded samples.

To determine the maximum H_2 photogeneration rate, we studied the effect of the Pt loading experimentally for C-doped $CdIn_2O_4$, undoped $CdIn_2O_4$, and C-doped In_2O_3 (Figure 4). The samples were prepared with loadings from 0.15% to 0.35% by wt in increments of 0.05%. Carbon-doped and undoped $CdIn_2O_4$ produced similar trends, in which the amount of hydrogen generated increased as the loading of platinum increased to 0.25 wt % and then began to decrease with an increase in loading. The C-doped In_2O_3 produced a much less defined optimum loading, though 0.20 wt % led to the greatest H_2 generation rate.

C-doped $CdIn_2O_4$ produced the most H_2 with a generation rate of 22,000 μmol h^{-1} $g_{catalyst}{}^{-1}$. Undoped $CdIn_2O_4$, C-doped In_2O_3 and CdO each produced successively lower production rates of 10,500, 5,700 and 2,600 μmol h^{-1} $g_{catalyst}{}^{-1}$, respectively. The increase in H_2 generation rate can be attributed to the introduction of Cd and C into the In_2O_3 lattice which led to a decrease in band gap and increase in absorption, respectively, and therefore an increase in the number of charge carriers available for reaction. It is possible that C-doping resulted in the formation of oxygen vacancies, which are required to compensate for the introduction of the anion dopant.[31] This would explain why no further band gap narrowing was observed after C-doping, only increased absorption.

The H_2 production rates for platinized C-doped $CdIn_2O_4$, undoped $CdIn_2O_4$, C-doped In_2O_3 were also compared to 0.3 wt % platinized TiO_2 (P-25 from Degussa), prepared by the same method.[24] The TiO_2 sample was analyzed with and without methanol (10 vol %) as a sacrificial reagent. Figure 5 shows the comparison of the H_2 generation plots. The TiO_2

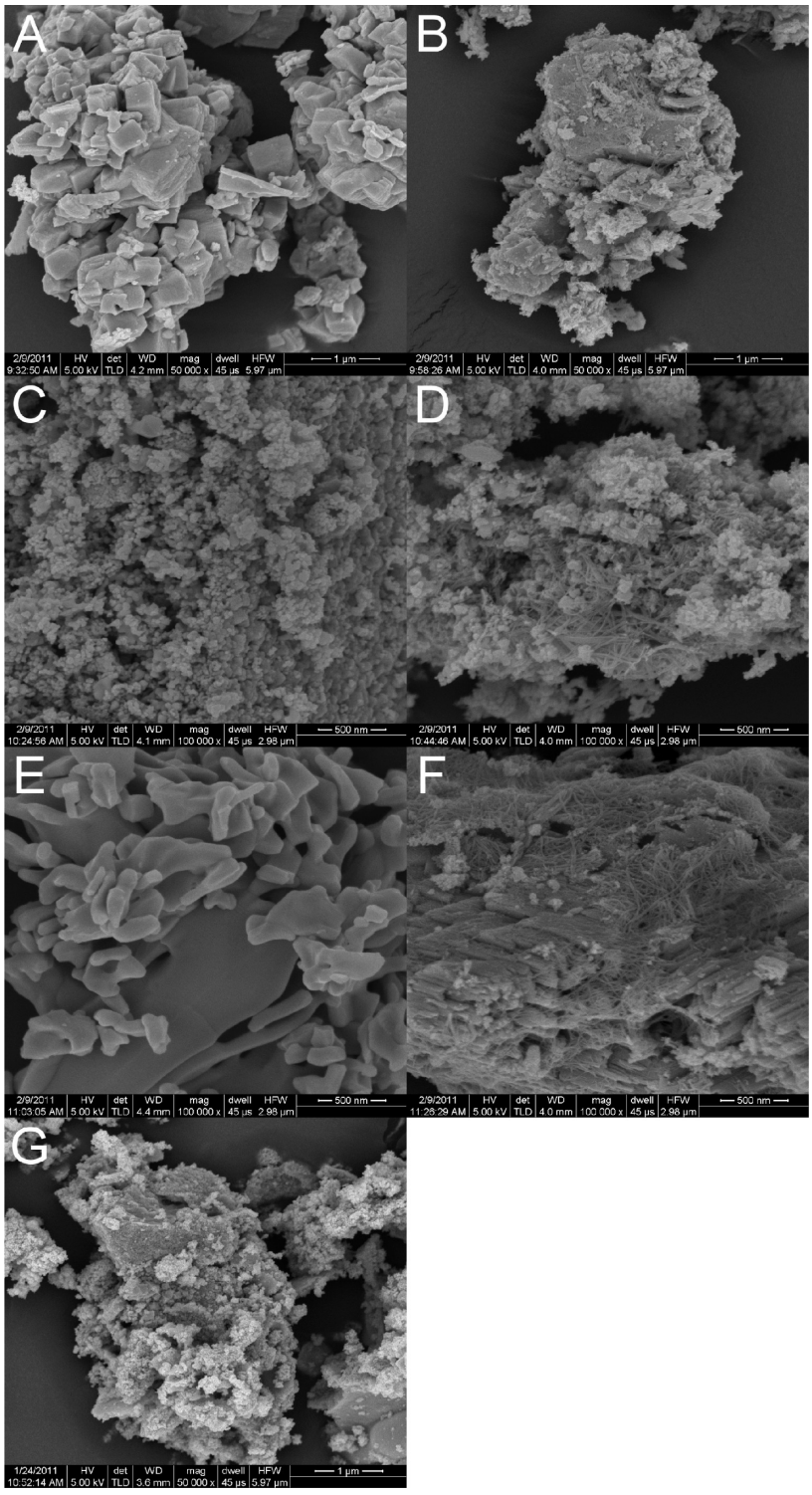

Figure 3. Scanning electron microcopy images of (A) $CdIn_2O_4$, (B) Pt:$CdIn_2O_4$, (C) C-$CdIn_2O_4$, (D) Pt:C-$CdIn_2O_4$, (E) CdO, (F) Pt:CdO, and (G) Pt:C−In_2O_3.

samples showed approximately a 2.5-fold increase in generation rate, from 2,100 to 5,400 μmol h^{-1} g^{-1} with the addition of methanol. Other studies report a H_2 generation rate in the range of 5,000−8,000 μmol h^{-1} g^{-1} over Pt/P-25 with a 0.3 wt % loading and using a 10 vol% methanol solution, which are in agreement with our measured value.[24,32] The rate of H_2 production in water for Pt-loaded C-doped $CdIn_2O_4$ rate is approximately four times greater than that of Pt-TiO_2 in a water/methanol solution under the same conditions and 10-fold greater than for Pt-TiO_2 in water alone. The ratio of evolved H_2 molecules to Pt atoms was determined to be 2,600, which is well above the required value to show that H_2 evolution from C-$CdIn_2O_4$ is a catalytic process. Similar calculations show that the ratios for H_2 evolution compared to Cd, In, and O are also above 1. The H_2 generation rates of all

dx.doi.org/10.1021/am300093t | ACS Appl. Mater. Interfaces 2012, 4, 2426−2431

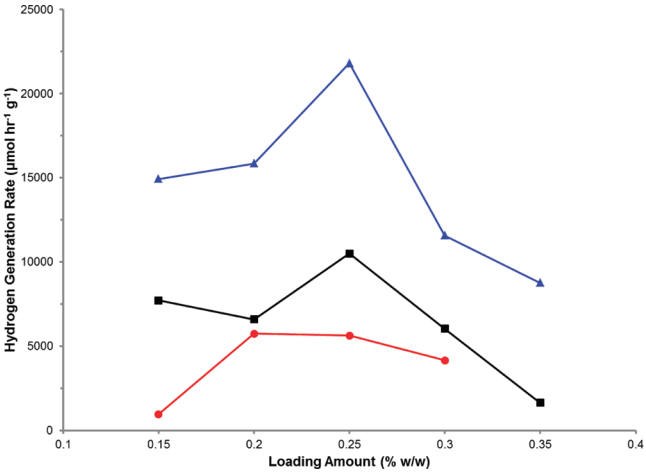

Figure 4. Platinum cocatalyst loading plot (by mass) for (▲) C-$CdIn_2O_4$, (■) $CdIn_2O_4$, and (●) C–In_2O_3.

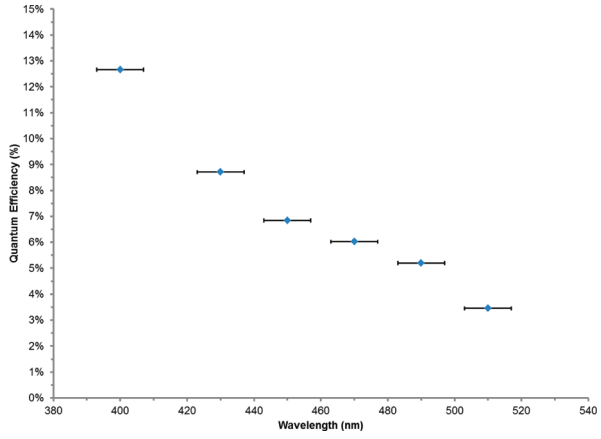

Figure 6. Quantum efficiency plotted as a function of wavelength for Pt-loaded C-doped $CdIn_2O_4$ using several bandpass filters.

materials were consistent between multiple runs, indicating the material is stable.

The quantum efficiency of the optimized Pt-loaded C-doped $CdIn_2O_4$ was measured as a function of wavelength using a series of bandpass filters and irradiating an excess mass of sample (~1.0 g). The resulting H_2 was measured in the same manner as the previous experiments. The apparent quantum efficiency (Φ) was calculated using the following equation:[33]

$$\Phi\ (\%) = (\text{no. of } H_2 \text{molecules} \times 2/\text{no. of incident photons}) \times 100\%$$

The number of incident photons was calculated using the measured power output of the lamp through each filter. The center wavelength was used to represent the input wavelength. The measured H_2 production rate was substituted for the total number of evolved H_2 molecules and the total number of incident photons was replaced with the photon flux. Figure 6 shows the quantum efficiency per wavelength of Pt-loaded C-doped $CdIn_2O_4$ (0.25 wt %). The quantum efficiency was measured for each of the following center wavelength regions: 400, 430, 450, 470, 490, and 510 nm, with the range never exceeding ±8 nm. The highest efficiency measured was 12.7% at 400 nm. The efficiency steadily dropped off at longer wavelengths; however H_2 production was still present out past 500 nm. Efficiency measurements were completed out to 510 nm but based on the UV–vis absorption data (Figure 2) the material should continue to produce H_2 as far into the visible as 600 nm. In comparison to Domen et al.,[34] who also reported wavelength studies for their $(Ga_{1-x}Zn_x)(N_{1-x}O_x)$ material, the H_2 production efficiency at 400 nm was 2.8% and dropped to 0% around 510 nm. However, at 510 nm, C-doped $CdIn_2O_4$ still is able to generate H_2. The efficiency of the material is a result of the effective separation of electron hole pairs. It has been documented that a cocatalyst is required to promote separation of the photoinduced charges by acting as an electron collector and assisting the surface reactions by providing active sites for H^+ reduction.[35,36] The separation of charges is enhanced by the cocatalyst loading due to the formation of a Schottky barrier at the semiconductor–metal interface, which results from the difference in work functions.[37]

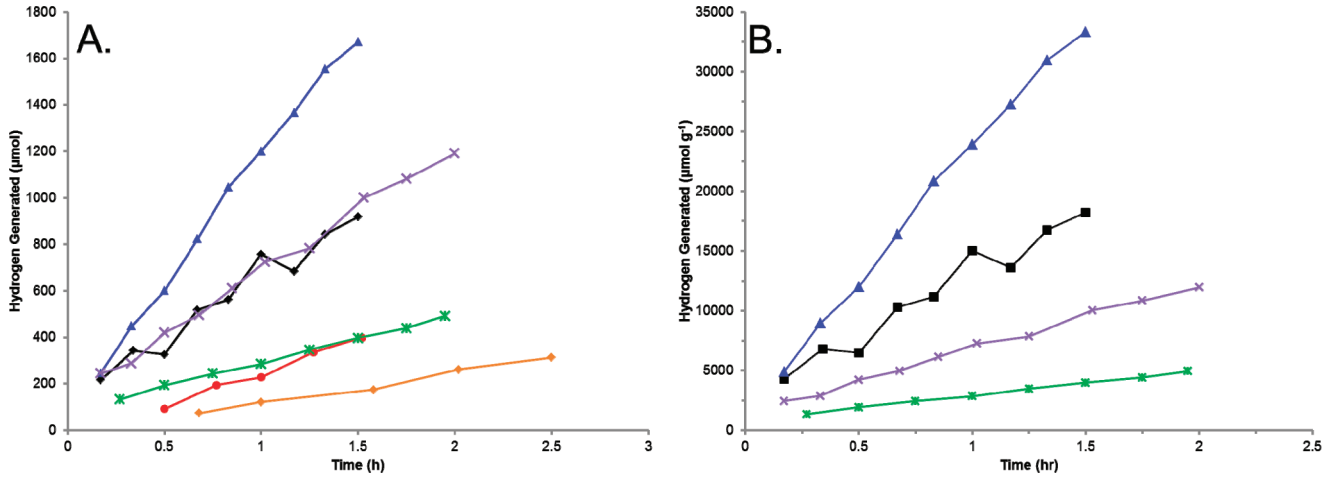

Figure 5. Comparison of H_2 generation plots for various photocatalytic materials. (A) Measured hydrogen amounts versus time, (B) Plots normalized to the amount of catalyst used. All In containing materials were measured using the optimized Pt loading amount. (▲) C-$CdIn_2O_4$, (■) $CdIn_2O_4$, (●) C–In_2O_3, (◆) CdO (*) TiO_2, and (X) TiO_2 suspended in a 10% (v/v) H_2O:MeOH solution. Linear fits to the data not shown for clarity purposes.

dx.doi.org/10.1021/am300093t | ACS Appl. Mater. Interfaces 2012, 4, 2426–2431

CONCLUSION

In summary, we have shown that Pt-loaded $CdIn_2O_4$ doped with carbon showed a high H_2 generation rate (22,000 μmol h^{-1} g^{-1}) and was over 2-fold greater than the undoped catalyst (10,500 μmol h^{-1} g^{-1}). The rate for the C-doped material was approximately 4-fold higher than Pt-TiO_2, and more importantly did not require a sacrificial agent. Quantum efficiency experiments showed the highest efficiency of the material to be 12.7% at 400 nm but this is reduced with increasing wavelength, as expected. Near 430 nm, the material was measured to have an efficiency of 8.7%. Using only 510 nm light, the material is still able to produce measurable amounts of H_2. The overall efficiency of the material is a promising step toward the development of efficient H_2 production water splitting catalysts.

AUTHOR INFORMATION

Corresponding Author

*E-mail: raftery@purdue.edu.

Notes

The authors declare no competing financial interest.

ACKNOWLEDGMENTS

Support for this work from the National Science Foundation (DMR-0805096) is gratefully acknowledged. The authors thank Debra M. Sherman for her assistance in acquisition of the SEM images and to Professor K. Choi for the diffuse reflectance measurements. D.R. is a member of the Purdue Energy Center.

REFERENCES

(1) Gratzel, M. *Nature* **2001**, *414*, 338−344.
(2) Cho, A. *Science* **2010**, *329*, 786−787.
(3) Nowotny, J.; Sorrell, C. C.; Sheppard, L. R.; Bak, T. *Int. J. Hydrogen Energy* **2005**, *30* (5), 521−544.
(4) Fujishima, A.; Honda, K. *Nature* **1972**, *238*, 37−38.
(5) Ahn, K.-S.; Yan, Y.; Lee, S.-H.; Deutsch, T.; Turner, J.; Tracy, C. E.; Perkins, C. L.; Al-Jassim, M. *J. Electrochem. Soc.* **2007**, *154*, B956−B959.
(6) Frites, M.; Shaban, Y. A.; Khan, S. U. M. *Int. J. Hydrogen Energy* **2010**, *35*, 4944−4948.
(7) Sivula, K.; Zboril, R.; Le Formal, F.; Robert, R.; Weidenkaff, A.; Tucek, J.; Frydrych, J.; Grätzel, M. *J. Am. Chem. Soc.* **2010**, *132*, 7436−7444.
(8) Sun, Y.; Murphy, C. J.; Reyes-Gil, K. R.; Reyes-Garcia, E. A.; Thornton, J. M.; Morris, N. A.; Raftery, D. *Int. J. Hydrogen Energy* **2009**, *34*, 8476−8484.
(9) McDonald, K. J.; Choi, K.-S. *Chem. Mater.* **2011**, *23*, 4863−4869.
(10) Li, W.; Li, J.; Wang, X.; Ma, J.; Chen, Q. *Int. J. Hydrogen Energy* **2010**, *35*, 13137−13145.
(11) Hossain, F. M.; Evteev, A. V.; Belova, I. V.; Nowotny, J.; Murch, G. E. *Comput. Mater. Sci.* **2010**, *48*, 854−858.
(12) Allam, N. K.; Grimes, C. A. *Sol. Energy Mater. Sol. Cells* **2008**, *92*, 1468−1475.
(13) Maeda, K.; Xiong, A.; Yoshinaga, T.; Ikeda, T.; Sakamoto, N.; Hisatomi, T.; Takashima, M.; Lu, D.; Kanehara, M.; Setoyama, T.; Teranishi, T.; Domen, K. *Angew. Chem., Int. Ed.* **2010**, *49*, 4096−4099.
(14) Robinson, D. M.; Go, Y. B.; Greenblatt, M.; Dismukes, G. C. *J. Am. Chem. Soc.* **2010**, *132*, 11467−11469.
(15) Pijpers, J. J. H.; Winkler, M. T.; Surendranath, Y.; Buonassisi, T.; Nocera, D. G. *Proc. Nat. Acad. Sci. U.S.A.* **2011**, *108*, 10056−10061.
(16) Asahi, R.; Morikawa, T.; Ohwaki, T.; Aoki, K.; Taga, Y. *Science* **2001**, *293*, 269−271.
(17) Kato, H.; Kudo, A. *J. Phys. Chem. B* **2002**, *106*, 5029−5034.
(18) Reyes-Gil, K. R.; Sun, Y.; Reyes-García, E.; Raftery, D. *J. Phys. Chem. C* **2009**, *113*, 12558−12570.
(19) Khan, S. U. M.; Al-Shahry, M.; Ingler, W. B. *Science* **2002**, *297*, 2243−2245.
(20) Iwashina, K.; Kudo, A. *J. Am. Chem. Soc.* **2011**, *133* (34), 13272−13275.
(21) Ikarashi, K.; Sato, J.; Kobayashi, H.; Saito, N.; Nishiyama, H.; Inoue, Y. *J. Phys. Chem. B* **2002**, *106*, 9048−9053.
(22) Sun, Y.; Thornton, J. M.; Morris, N. A.; Rajpura, R.; Henkes, S.; Raftery, D. *Int. J. Hydrogen Energy* **2011**, *36*, 2785−2793.
(23) Ali, H. M.; Mohamed, H. A.; Wakkad, M. M.; Hasaneen, M. F. *Thin Solid Films* **2007**, *515*, 3024−3029.
(24) Sreethawong, T.; Yoshikawa, S. *Int. J. Hydrogen Energy* **2006**, *31*, 786−796.
(25) Cahen, D.; Ibers, J. A.; Mueller, M. H. *Inorg. Chem.* **1974**, *13*, 110−115.
(26) Patterson, A. L. *Phys. Rev.* **1939**, *56*, 978.
(27) Karvaly, B.; Hevesy, I. *Z. Naturforsch., A* **1971**, *26*, 245.
(28) Kammler, D. R.; Mason, T. O.; Poeppelmeier, K. R. *Chem. Mater.* **2000**, *12*, 1954−1960.
(29) Pisarkiewicz, T.; Zakrzewska, K.; Leja, E. *Thin Solid Films* **1987**, *153*, 479−486.
(30) Mulligan, W. P. In *A Study of the Fundamental Limits to Electron Mobility in Cadmium Stannate Thin Films*; Colorado School of Mines: Golden, CO, 1997.
(31) Batzill, M.; Morales, E. H.; Diebold, U. *Phys. Rev. Lett.* **2006**, *96*, 026103.
(32) Yi, H.; Peng, T.; Ke, D.; Ke, D.; Zan, L.; Yan, C. *Int. J. Hydrogen Energy* **2008**, *33*, 672−678.
(33) Maeda, K.; Teramura, K.; Takata, T.; Hara, M.; Saito, N.; Toda, K.; Inoue, Y.; Kobayashi, H.; Domen, K. *J. Phys. Chem. B* **2005**, *109*, 20504−20510.
(34) Maeda, K.; Teramura, K.; Lu, D.; Takata, T.; Saito, N.; Inoue, Y.; Domen, K. *Nature* **2006**, *440*, 295−295.
(35) Inoue, Y. *Energy Environ. Sci.* **2009**, *2*, 364−386.
(36) Maeda, K.; Higashi, M.; Lu, D.; Abe, R.; Domen, K. *J. Am. Chem. Soc.* **2010**, *132*, 5858−5868.
(37) Liang, Y.-C.; Wang, C.-C.; Kei, C.-C.; Hsueh, Y.-C.; Cho, W.-H.; Perng, T.-P. *J. Phys. Chem. C* **2011**, *115*, 9498−02.